

Three-Dimensional Topological Insulator in a Magnetic Field: Chiral Side Surface States and Quantized Hall Conductance

Yan-Yang Zhang,¹ Xiang-Rong Wang,² and X.C. Xie³

¹*Department of Physics and Center of Computational and Theoretical Physics,
The University of Hong Kong, Pokfulam Road, Hong Kong*

²*Department of Physics, The Hong Kong University of Science and Technology, Clear Water Bay,
Kowloon, Hong Kong and School of Physics, Shandong University, Jinan, P. R. China*

³*International Center for Quantum Materials, Peking University,
Beijing, China 100083 and Department of Physics,
Oklahoma State University, Stillwater, OK 74078*

(Dated: January 15, 2013)

Low energy excitation of surface states of a three-dimensional topological insulator (3DTI) can be described by Dirac fermions. By using a tight-binding model, the transport properties of the surface states in a uniform magnetic field is investigated. It is found that chiral surface states parallel to the magnetic field are responsible to the quantized Hall (QH) conductance $(2n+1)\frac{e^2}{h}$ multiplied by the number of Dirac cones. Due to the two-dimension (2D) nature of the surface states, the robustness of the QH conductance against impurity scattering is determined by the oddness and evenness of the Dirac cone number. An experimental setup for transport measurement is proposed.

PACS numbers: 71.70.Di, 72.10.-d, 73.20.At, 73.43.-f

I. INTRODUCTION

Topological insulator (TI), a new quantum state in which the bulk is an insulator and the surface is metallic, has attracted intensive attention[1] since its theoretical predictions[2–4] and its experimental realizations[5–8] in three dimensions. Unlike normal insulators, the boundary (edges or surfaces) of a finite TI sample supports extended and current carrying states in its bulk gap. In the presence of time reversal symmetry, TIs can be classified by a \mathbb{Z}_2 invariant integer ν [9–11] into a weak TI for even number of the Dirac cones (called $\nu = 1$) and a strong TI for odd number of the Dirac cones (called $\nu = -1$). The edge/surface states of a weak (strong) TI can (cannot) be destroyed by defect scatterings[2, 3].

The surface states of a three-dimensional topological insulator (3DTI) are described by two-dimensional (2D) Dirac cones centered at the time-reversal invariance points in the Brillouin zone. 2D Dirac fermions with a single cone are predicted to have many novel properties such as the Klein paradox, anti-localization, etc.[12–15] In the quantum Hall effect (QHE) regime (strong magnetic field), the Landau levels of a single cone Dirac fermion is unevenly distributed

$$E_n \sim \sqrt{B|n|}, \quad n = 0, \pm 1, \pm 2, \dots \quad (1)$$

This distribution has been confirmed by several experiments[16–18]. Another interesting prediction of one Dirac cone fermion is the *half* (in the unit of e^2/h) quantized Hall (QH) conductance[14, 19, 20] because one Dirac cone carries a π Berry phase. Although many properties of strong 3DTIs have been confirmed since its experimental realization in several semiconductors, the half QH conductances has not been observed in experiments

yet, and this will be our focus.

In this paper, we investigate a 3DTI in a uniform magnetic field within a well-known tight binding model. Our calculations yield indeed the well-known Landau levels (Eq. (1)). However, the issue of the half QH conductance is subtle. All surface states of a finite 3DTI are fully connected with each other[2, 3, 21] and surface states living on the sample surface may move from one side to another. In other words, the well-defined Hall voltage measurement in usual 2D electron gases (2DEG) is not so clear in the 3DTI cases since two surfaces cannot be separated by the bulk of a finite 3DTI as it did in 2D QHE systems. The current does not come from 1D channels, but from 2D surface states. The structures of these side surface states are more complicated than the edge states in 2DEG, therefore well-defined quantum Hall plateaus $(2n+1)\frac{e^2}{h}$ can only be defined from transverse current instead of the Hall voltage. Our tight-binding calculations confirm the earlier predictions based on an effective theory of Dirac fermion in curved 2D spaces[21]. The robustness of the Hall conductance against impurities is also studied. Our tight-binding model and their basic properties are introduced in the next section. Numerical results and their discussions are presented in section III, followed by the conclusion section.

II. MODEL

A well-known tight-binding model of 3DTI[22] is

$$H_0(\mathbf{k}) = \epsilon_0(\mathbf{k})I_{4 \times 4} + \sum_{a=1}^5 d_a(\mathbf{k})\Gamma^a$$

$$d_a(\mathbf{k}) = (A_2 \sin k_x, A_2 \sin k_y, A_1 \sin k_z, \mathcal{M}(k), 0), \quad (2)$$

where $\epsilon_0(\mathbf{k}) = C + 2D_1 + 4D_2 - 2D_1 \cos k_z - 2D_2(\cos k_x + \cos k_y)$, $\mathcal{M} = M - 2B_1 - 4B_2 + 2B_1 \cos k_z + 2B_2(\cos k_x + \cos k_y)$ and $\Gamma^{1,2,3,4,5} = (\sigma_x \otimes s_x, \sigma_x \otimes s_y, \sigma_y \otimes I_{2 \times 2}, \sigma_z \otimes I_{2 \times 2}, \sigma_x \otimes s_z)$ in the basis of four states ($|P1_z^+, \uparrow\rangle, |P1_z^+, \downarrow\rangle, |P2_z^-, \uparrow\rangle, |P2_z^-, \downarrow\rangle$). After inverse Fourier transformation of equation (2), the real space version of this model on a cubic lattice can be written in the form

$$H_0 = \sum_{is} \epsilon_{is} c_{is}^\dagger c_{is} + \sum_{\langle ij \rangle ss'} t_{ij}^{ss'} c_{is}^\dagger c_{js'} + \text{H.c.}, \quad (3)$$

where i, j are lattice site indices, $s \in \{|P1_z^+, \uparrow\rangle, |P1_z^+, \downarrow\rangle, |P2_z^-, \uparrow\rangle, |P2_z^-, \downarrow\rangle\}$ is the spin-orbital index. The first term in equation (3) is the on-site energy, the second and third terms describe the hoppings between nearest neighbor sites. The effect of non-magnetic impurities can be included by adding a term

$$H_I = \sum_{is} V_{is} c_{is}^\dagger c_{is}, \quad (4)$$

where V_{is} distributes randomly in the energy range of $(-W/2, W/2)$. The magnetic field \mathbf{B} is introduced through the Peierls substitution of hopping coefficients[23, 24]

$$t_{ij}^{ss'} \rightarrow \exp\left(\frac{2\pi i}{\phi_0} \int_i^j d\mathbf{l} \cdot \mathbf{A}\right) t_{ij}^{ss'}, \quad (5)$$

where $\phi_0 = e/h$.

In the clean limit ($H_I = 0$), this 3D model is fully gapped in the energy range $(-M, M)$. The properties of surface states within this gap are determined by the \mathbb{Z}_2 topological numbers related to the time reversal polarizations[2, 3, 9]

$$\delta_i = \frac{\sqrt{\det[w(\Gamma_i)]}}{\text{Pf}[w(\Gamma_i)]} = -\text{sgn}(d_4(\mathbf{k} = \Gamma_i)) = \pm 1, \quad (6)$$

at 8 time-reversal invariant points in the first Brillouin zone: $\Gamma_{1,2,3,4,5,6,7,8} = (0, 0, 0), (\pi, 0, 0), (0, \pi, 0), (0, 0, \pi), (0, \pi, \pi), (\pi, 0, \pi), (\pi, \pi, 0), (\pi, \pi, \pi)$, where $w_{mn}(\mathbf{k}) \equiv \langle u_{-\mathbf{k}, m} | \Theta | u_{\mathbf{k}, n} \rangle$. If $\nu \equiv \prod_{i=1}^8 \delta_i = -1$, the system is a strong 3DTI with odd numbers of the Dirac cones on *each* surface. Otherwise, the system ($\nu = 1$) is a weak 3DTI with even numbers of the Dirac cones on each surface. In terms of model parameters, the system is in a strong (weak) TI phase when $B_i/M > 1$ ($B_i/M < -1$)[2].

The surface states around each Dirac cone is approximately described by the Dirac fermion Hamiltonian (z -axis is normal to the surface)[4, 14, 22, 25]

$$H_{xy} = v_F(\sigma_x k_y - \sigma_y k_x), \quad (7)$$

with a linear dispersion relation

$$E_{xy} = \pm v_F \sqrt{k_x^2 + k_y^2}, \quad (8)$$

where $v_F = A_2 \sqrt{1 - (\frac{D_1}{B_1})^2}$ and $\hbar = 1$ is adopted.

Before presenting calculations of tight binding models, let us first look at effective model (Eq. (7)) in a field $\mathbf{B} = (0, 0, B)$ perpendicular to the surface. In the Landau gauge $\mathbf{A} = (-By, 0, 0)$, H_{xy} is[13]

$$H_{xy} = v_F[\sigma_x(k_y - A_y) - \sigma_y(k_x - A_x)] \\ = v_F \begin{pmatrix} 0 & k_y + i(k_x + eBy) \\ k_y - i(k_x + eBy) & 0 \end{pmatrix}, \quad (9)$$

where $k_i = -i\partial_i$. The eigenvalues are Landau levels [13]

$$E_{xy} = \pm v_F \sqrt{2neB}, \quad n = 0, 1, 2, \dots \quad (10)$$

However, for surface parallel to magnetic field, say, $x-z$ plane, the Hamiltonian is

$$H_{xz} = \sigma_x(p_z - A_z) - \sigma_y(p_x - A_x) \quad (11)$$

$$= \begin{pmatrix} 0 & p_z + i(p_x + eBy) \\ p_z - i(p_x + eBy) & 0 \end{pmatrix}. \quad (12)$$

Since eBz commutes with k_x and k_y , the only difference between Eq. (12) and Eq. (7) is a shift $-eBy$ of the Dirac point in k_x direction. The eigenvalue shows a shifted Dirac cone

$$E_{xz} = \pm v_F \sqrt{(k_x + eBy)^2 + k_z^2}. \quad (13)$$

We will see that states in the surfaces parallel to the magnetic field play an important role in the QHE in 3DTI.

III. NUMERICAL RESULTS

To be specific, we consider Hamiltonian (3) on a cubic lattice with size $N_x \times N_y \times N_z$. For a slab $\infty \times \infty \times N_z$ of thickness N_z in z -direction and infinite in other two directions[3], the surface states of the TI can be displayed by plotting the dispersion relation $E(k_x, k_y)$ inside the bulk gap so that this dispersion relation must be from the surface states. Fig. 1 (a) is the dispersion relation of a slab without a magnetic field. The Dirac cone can be clearly seen. There are two degenerated Dirac cones located on lower ($z = 1$) and upper ($z = N_z$) surfaces, respectively. The existence of such surface states roots on the topological property of time reversal symmetric systems[2, 9]. The magnetic field breaks time reversal symmetry and the fate of surface states will be tested in the following tight-binding calculation. A uniform magnetic field generally also breaks the lattice translational symmetry[26] and results in the Hofstadter butterfly spectrum[27]. If the magnetic flux through a unit cell is a fraction of the flux quanta, $Ba^2 = \frac{p}{q}\phi_0$, where p and q are two prime numbers and a is the lattice constant, periodic structure is

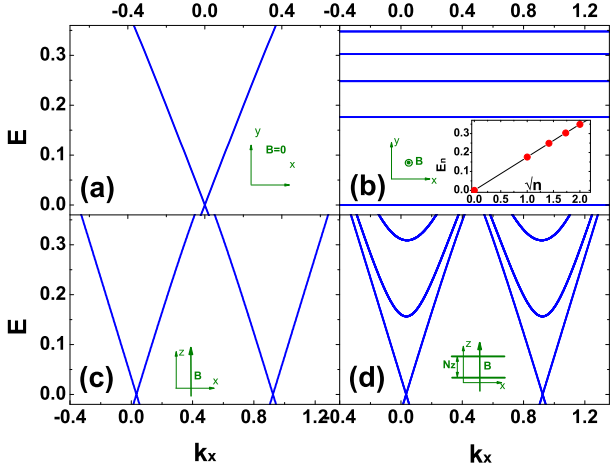


FIG. 1: (Color online) Dissipation relations of a strong 3DTI with model parameters $A_1 = A_2 = 1$, $B_1 = B_2 = 1$, $C = 0$, $D_1 = D_2 = 0$ and $M = 0.4$. (a): $E(k_x, k_y = 0)$ for a slab with geometry $\infty \times \infty \times 40$ and without magnetic field. (b): Similar to (a), but in a perpendicular magnetic field $B_z = \frac{\phi_0}{400a^2}$. Inset of (b): the Landau levels E_n versus \sqrt{n} . (c): $E(k_x, k_z = 0)$ for a slab with geometry $\infty \times 60 \times \infty$ in a parallel magnetic field $B_z = \frac{\phi_0}{400a^2}$. (d) $E(k_x)$ for a bar of $\infty \times 60 \times 40$ with periodic boundary condition in z direction, in a magnetic field $B_z = \frac{\phi_0}{400a^2}$, in contrast to its infinite-size version (c).

restored with an enlarged and y -elongated unit cell of q -times of the original one, $a'_x = a_x$ and $a'_y = qa_y$, then $k_x \in [-\pi/a, \pi/a]$ and $k_y \in [-\pi/(qa), -\pi/(qa)]$ are good quantum numbers[28, 29]. Fig. 1 (b) is the dispersion relation of the same slab as that for Fig. 1 (a) in a perpendicular magnetic field $\mathbf{B} = (0, 0, B)$. Instead of linear dispersion relation in zero field, discrete Landau levels E_n appear. We have confirmed that there are an upper-lower surface double degeneracy and all wavefunctions are strongly confined inside (top/bottom) surfaces. Although the time-reversal symmetry is broken, the magnetic field does not destroy the 2D nature of the surface states. The dependence $E_n \sim \sqrt{n}$ is also verified as shown in the inset of Fig. 1 (b). Such Landau levels have already been observed in recent experiments[17, 18].

We plot also the dispersion relation for the infinite $x-z$ surfaces in a parallel magnetic field $\mathbf{B} = (0, 0, B)$ in Fig. 1 (c). Shifted Dirac cones corresponding to two surfaces ($y = 1$ and $y = N_y$) can be clearly seen, as predicted in Eq. (13). We will see that these side surface states play an important role in the following discussion. Fig. 1 (d) is similar to (c) when the infinite surface is confined along z -direction with a periodic boundary condition that eliminates possible edge states. Subband structures appear seen due to the z -confinement.

With quantized Landau levels, one naturally expects quantum Hall effects. In conventional 2DEGs, quantized Hall conductance comes from the spatially separated counter-propagating edge channel(s) on the two

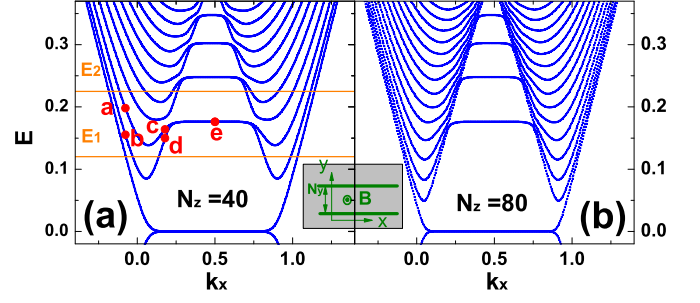


FIG. 2: (Color online) Dissipation relation $E(k_x)$ along the x -direction of a bar geometry $\infty \times 60 \times N_z$ in a perpendicular magnetic field $B_z = \frac{\phi_0}{400a^2}$: (a) $N_z = 40$; and (b) $N_z = 80$. Other model parameters are identical to that for Fig. 1.

sides of a samples[30]. The situation in 3D is subtle because a surface state may cover all surfaces because they are fully connected[2, 3, 21]. In other words, a surface state cannot be confined on only one surface, resulting in more interesting with richer physics.

To study possible current carrying surface states, we consider a bar geometry of finite widths of N_y and N_z in both y - and z - directions. The dispersion relation along x -direction in a magnetic field is plotted in Fig. 2. The constant energy in the middle of the curves shows that the Landau levels exist in the middle of the surface. The Landau levels float up near the edges (junctions of two surfaces). We have confirmed that the left-most ($k_x < 0.1$) and right-most ($k_x > 0.8$) parts of the curves correspond to states distributed mostly on the left ($y = 1$) and the right ($y = N_y$) side surfaces, respectively (Fig. 3). These side surface states are spin-polarized due to spin-orbit coupling[21], as plotted in Fig. 4.

As illustrated in Fig. 3(a) to (e), varying k_x from either side of the curves to the middle flat parts, the states move from the side surfaces of $y = 1$ and $y = N_y$ (Fig. 1 (d)), to the top and bottom surfaces of $z = 1$ and $z = N_z$ (Fig. 1 (b)) continuously. This is possible because a particle can move from the side surfaces to the top/bottom ones without passing through the bulk. In other words, the surface states live essentially on a closed surface of a finite 3DTI sample. One cannot have 1D edge channels as in the 2D case. The discreteness of these states simply originates from the finite thickness N_z in z -direction, as indicated in Fig. 2 (a) and (b). Increasing N_z does not affect the Landau levels, but generates more side surface-state subbands. In the limit of large N_z , these subbands pack densely and form two continuum cones, similar to the shifted Dirac cones in parallel magnetic field in Fig. 1 (c).

Similar to edge states in conventional 2D systems, due to non-zero dispersion, the side surface states can transport electrons in the presence of voltage along x direction. The effects of side surface states have been noticed in a recent transport measurement[31]. However,

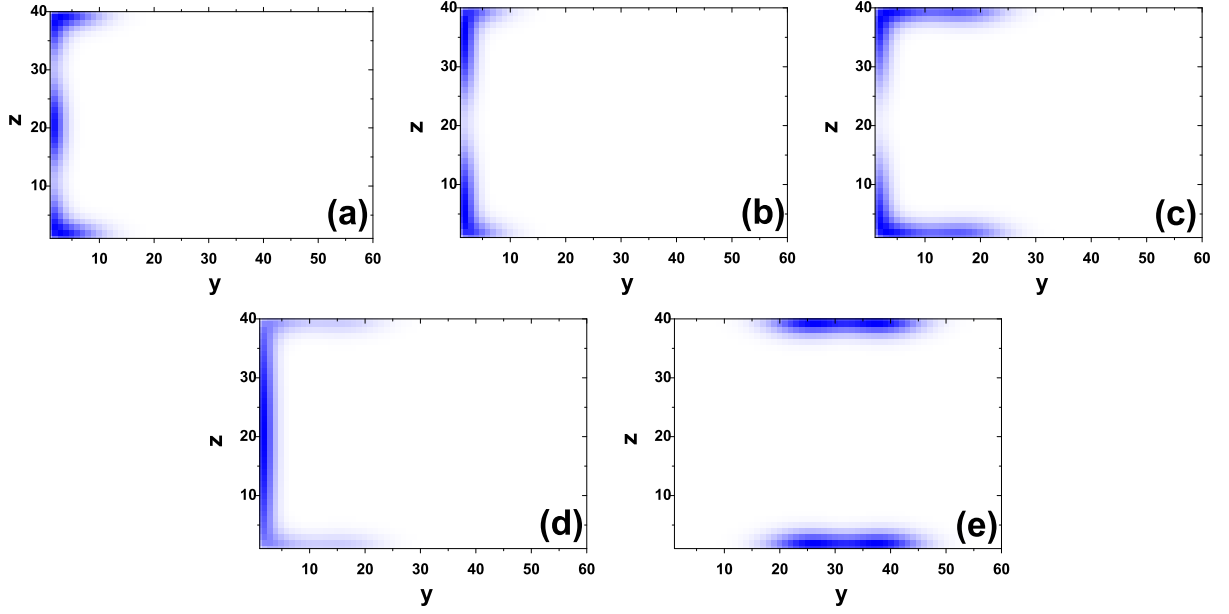


FIG. 3: (Color online) Spatial distributions of wavefunctions on the $y - z$ section of the bar for the states marked as red dots in Fig. 2 (a). The magnetic field is in z -direction. (a) to (e) corresponds to state points a to e, respectively.

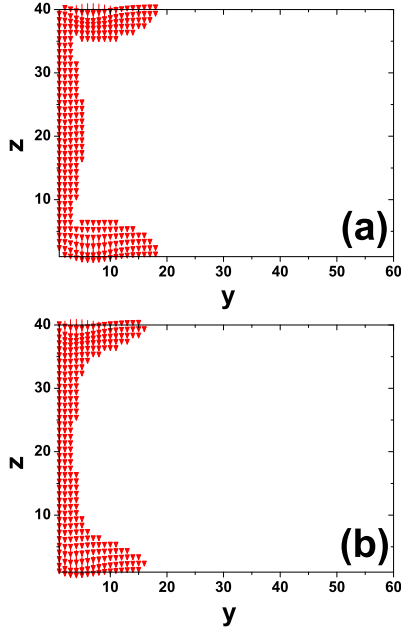


FIG. 4: (Color online) Spatial distributions of local spin s_z . (a) and (b) correspond to state points a and b in Fig. 2, respectively.

the side surface states are quite different from the edge states in 2DEG. For example, the dependence of $E_n(k_x)$ is non-monotonic on each side. This brings the coexistence of both forward and backward moving channels on each side, as illustrated in Fig. 5. At each side and for a given energy, the numbers of forward moving channels n_f

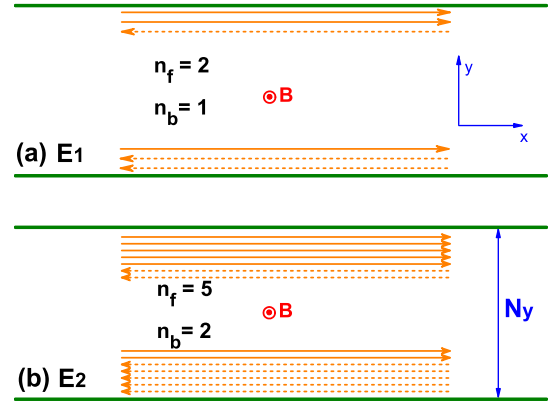


FIG. 5: (Color online) Schematic drawing (seen from above) of the active side surface channels at the Fermi energies E_1 (a) and E_2 (b) indicated by the orange lines in Fig. 2 (a). The channel numbers of forward moving n_f and backward moving n_b are indicated.

and backward moving n_b depend on magnetic field B , as well as thickness N_z of the sample. However, their difference $n_f - n_b = 1, 3, 5, \dots$ is universal between any definite pair of adjacent Landau levels, as long as the dimension of the sample is not too small to couple states on any opposite surfaces[25]. A general theorem guarantees the existence of current carrying states[32]. The directions of these net currents on two sides are reversed, thus they are chiral. Experimentally, such chiral currents can be measured by a multi-terminal measurement illustrated in Fig. 6. In such setups, the Landauer-Büttiker formula

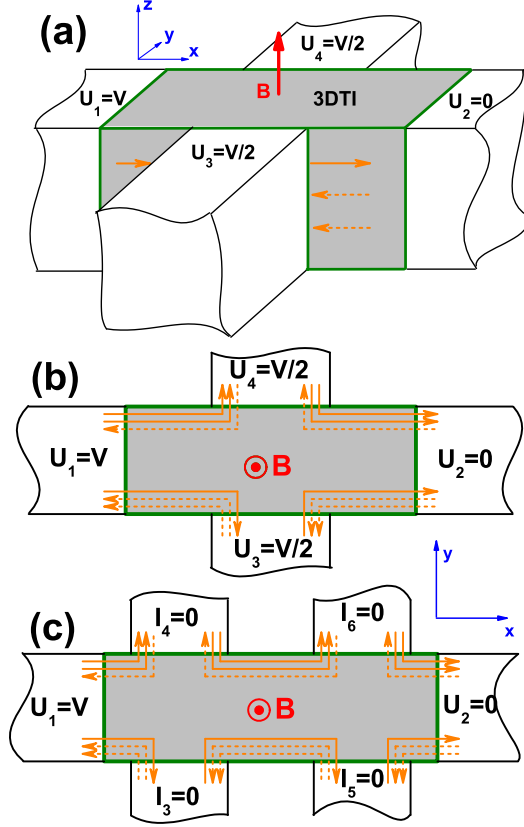


FIG. 6: (Color online) The schematic drawing of 3D multi-terminal measurements of the TI (grey). The uniform magnetic field B (red) is in the z -direction. The orange arrows represent the side surface channels that carry currents. (a) The 3D schematic diagram of a four-terminal measurement. A voltage V is applied to the left (1) and right (2) terminals. The potential of the front and back terminals are $V/2$ and $V/2$, respectively. (b) The vertical view of (a) from above. (c) The vertical view of a 3D six-terminal measurement, which is not preferred in our model.

is $I_j = \sum_i T_{j \leftarrow i} [V_j - V_i]$, where $T_{j \leftarrow i}$ is the transmission from lead i to lead j , V_i and I_i are the voltage and the current in the i -th lead respectively, satisfying Kirchoff's law $\sum_i I_i = 0$ [33]. In the clean limit, all the active channels are perfectly conducting and the transmission $T_{j \leftarrow i}$ can be read directly from the profile of the active surface channels, as shown in Fig. 6. For the four-terminal setup illustrated in Fig. 6 (a) and (b), straightforward calculations within this formalism give

$$G_{xy} \equiv \frac{I_3 - I_4}{V} = \frac{2I_3}{V} = -\frac{2I_4}{V} = (n_f - n_b) \frac{e^2}{h}, \quad (14)$$

$$G_{xx} \equiv \frac{I_1 - I_2}{V} = \frac{2I_1}{V} = -\frac{2I_2}{V} = (n_f + n_b) \frac{e^2}{h}. \quad (15)$$

This G_{xy} is the Hall conductance in the present problem. This is consistent with the previous calculation based on an effective model in curved space[21], but here understood within simple band theories. Similar results hold

for the case of surface states with more than one Dirac cones and the only difference is the conductance is multiplied by a factor of N_{cone} , the number of Dirac cones. However, for a 3D six-terminal setup, shown in Fig. 6 (c) and generalized from the traditional 2D Hall bar, similar calculations show that

$$G_{xy} = \frac{V_3 - V_4}{I_1} = \frac{n_b - n_f}{n_b^2 - n_b n_f + n_f^2} \cdot \frac{e^2}{h}, \quad (16)$$

$$G_{xx} = \frac{V_3 - V_5}{I_1} = \frac{n_b n_f}{n_b^3 + n_f^3} \cdot \frac{e^2}{h}, \quad (17)$$

which is generally sample dependent and not quantized.

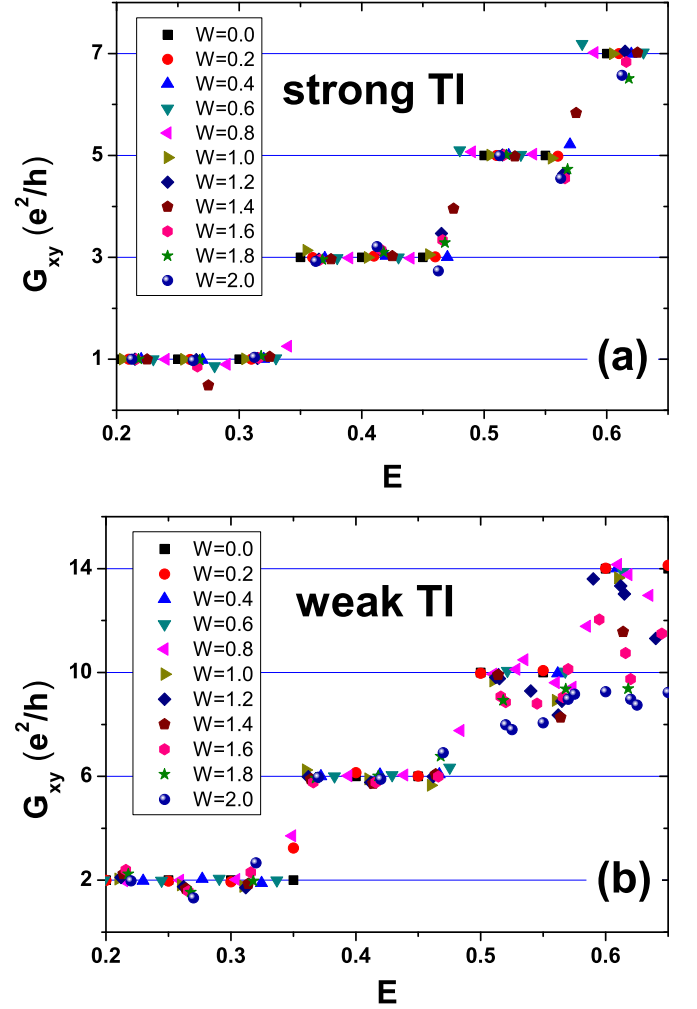


FIG. 7: (Color online) Hall conductance G_{xy} as a function of the Fermi energy E for various disorder strength W . G_{xy} for a strong (a) and weak TI (b) is calculated from a four-terminal setup as illustrated in Fig. 6. The sample size is 38×18 and the model parameters are $A_1 = A_2 = 1$, $B_2 = 1$, $C = 0$, $D_1 = D_2 = 0$, $M = 0.8$ and $B_1 = \pm 1$ for strong (weak) TI.

One question arises: is the value of the Hall conductance G_{xy} defined in Eq. (15) robust against disorder[34]? In zero magnetic field, it is well-known that

the surface states are robust for odd N_{cone} (strong TI) and not for even N_{cone} (weak TI). Since charge transport is dominated by the side surface states at zero field, it is reasonable to expect that the robustness of G_{xy} is also determined by the evenness and oddness of N_{cone} . Specifically, for strong TI with single-cone surface states in a magnetic field, as illustrated in Fig. 2, forward and backward channels coexist at the same side, but they originate from a single Dirac cone and the backscattering is small. These are confirmed by numerical simulations of a four-terminal set-up as shown in Fig. 7 (a) for a strong 3DTI and in Fig. 7 (b) for a weak 3DTI, by using the standard method of non-equilibrium Green's functions[33, 35]. In the weak TI case, the conductance G_{xy} is twice as large due to double cone degeneracy. Also, its value is sensitive to disorder because of the inter-scattering between the two cones. Since a four-terminal numerical simulation is very resource consuming, in Fig. 7 we use a smaller size system. The physics remains the same as long as no direct coupling between surface states on two opposite surfaces. Quantized Hall plateaus predicted from above analysis, especially for the strong TI, can be clearly seen. In the presence of disorder, the quantum Hall plateaus of a strong TI (Fig. 7 (a)) survive much better than those of a weak TI (Fig. 7 (b)).

IV. SUMMARY

Before ending this paper, it should be emphasized that we did not obtain the half conductance, or in a less strict sense, we saw the sum of half conductance from upper and lower surfaces[21], since the Dirac fermion live on a closed and curved surface of 3DTI. By making an *edge* channel on one surface, one inevitably makes a new one on the opposite surface so that a Dirac fermion will not terminate somewhere on a surface. The exact half Hall conductance of one surface cannot directly be observed unless the surface state can be effectively confined in one isolated plane by some means. On the other hand, the quantized Hall conductance we obtained from the 2D surface states should not be viewed as a trivial application of Chern number theory of 2DEG[28, 29], since the surface states live on a closed 2D manifold embedded in a 3D space, which is topologically different from the 2D plane of 2DEG.

In summary, we investigated the quantum Hall effect of a 3DTI in a magnetic field. The integer Hall conductance is carried by side surface states due to the non-separable nature of surface states enclosing the 3DTI. The quantum Hall conductance reflects the properties of side surface states that are parallel to the magnetic field. The quantum Hall effect thus offers a transport measurement to determine the topological property of a 3DTI: whether it is a weak or strong TI, the number of Dirac cones, etc.

ACKNOWLEDGEMENTS

XCX is supported by NSF-China, MOST-China and US-DOE-DE-FG-02-04ER46124. XRW is supported by HK CRF (No HKU10/CRF/08-HKUST17/CRF/08) and RGC grants.

-
- [1] M. Z. Hasan and C. L. Kane, Rev. Mod. Phys. **82**, 3045C3067 (2010) .
 - [2] L. Fu and C. L. Kane, Phys. Rev. B **76**, 045302 (2007).
 - [3] L. Fu, C. L. Kane and E. J. Mele, Phys. Rev. Lett. **98**, 106803 (2007).
 - [4] H. Zhang, C.-X. Liu, X.-L. Qi, X.- Dai, Z. Fang and S.-C. Zhang, Nat. Phys. **5**, 438 (2009).
 - [5] D. Hsieh, Y. Xia, D. Qian, L. Wray, J. H. Dil, F. Meier, J. Osterwalder, L. Patthey, J. G. Checkelsky, N. P. Ong, A. V. Fedorov, H. Lin, A. Bansil, D. Grauer, Y. S. Hor, R. J. Cava and M. Z. Hasan, Nature **460**, 1101 (2009).
 - [6] P. Roushan, J. Seo, C. V. Parker, Y. S. Hor, D. Hsieh, D. Qian, A. Richardella, M. Z. Hasan, R. J. Cava and A. Yazdani, Nature **460**, 1106 (2009).
 - [7] Y. L. Chen, J. G. Analytis, J.-H. Chu, Z. K. Liu, S.-K. Mo, X. L. Qi, H. J. Zhang, D. H. Lu, X. Dai, Z. Fang, S. C. Zhang, I. R. Fisher, Z. Hussain, Z.-X. Shen, Science **325**, 178 (2009).
 - [8] D. Hsieh, Y. Xia, D. Qian, L. Wray, F. Meier, J. H. Dil, J. Osterwalder, L. Patthey, A.V. Fedorov, H. Lin, A. Bansil, D. Grauer, Y. S. Hor, R. J. Cava and M. Z. Hasan, Phys. Rev. Lett. **103**, 146401 (2009).
 - [9] L. Fu and C. L. Kane, Phys. Rev. B **74**, 195312 (2006).
 - [10] J. E. Moore and L. Balents, Phys. Rev. B **75**, 121306(R) (2007).
 - [11] X.-L. Qi, T. L. Hughes and S.-C. Zhang, Phys. Rev. B **78**, 195424 (2008).
 - [12] M. I. Katsnelson, K. S. Novoselov and A. K. Geim, Nat. Phys. **2**, 620 (2006).
 - [13] N. H. Shon and T. Ando, J. Phys. Soc. Jpn. **67**, 2421 (1998).
 - [14] T. Ando, T. Nakanishi and R. Saito, J. Phys. Soc. Jpn. **67**, 2857 (1998).
 - [15] K. Nomura, M. Koshino and S. Ryu, Phys. Rev. Lett. **99**, 146806 (2007).
 - [16] T. Zhang, P. Cheng, X. Chen, J.-F. Jia, X. Ma, K. He, L. Wang, H. Zhang, X. Dai, Zh. Fang, X.-C. Xie, Q.-K. Xue, arXiv:0908.4136 (2009).
 - [17] P. Cheng, C. Song, T. Zhang, Y. Zhang, Y. Wang, J.-F. Jia, J. Wang, Y. Wang, B.-F. Zhu, X. Chen, X. Ma, K. He, L. Wang, X. Dai, Z. Fang, X. C. Xie, X.-L. Qi, C.-X. Liu, S.-C. Zhang, Q.-K. Xue, Phys. Rev. Lett. **105**, 076801 (2010).
 - [18] T. Hanaguri, K. Igarashi, M. Kawamura, H. Takagi, and T. Sasagawa, Phys. Rev. B **82**, 081305 (2010).
 - [19] K. S. Novoselov, E. Mccann, S. V. Morozov, V. I. Fal'Ko, M. I. Katsnelson, U. Zeitler, D. Jiang, F. Schedin And A. K. Geim, Nat. Phys. **2**, 177 (2006).
 - [20] D. Xiao, W. Yao and Q. Niu, Phys. Rev. Lett. **99**, 236809 (2007).
 - [21] D.-H. Lee, Phys. Rev. Lett. **103**, 196804 (2009).
 - [22] R. Li, J. Wang, X.-L. Qi and S.-C. Zhang, Nature Phys.

- 6**, 284 (2010).
- [23] X. R. Wang, Phys. Rev. B **53**, 12035(1996).
 - [24] J. Maciejko, X.-L. Qi and S.-C. Zhang, Phys. Rev. B **82**, 155310 (2010).
 - [25] W.-Y. Shan, H.-Z. Lu and S.-Q. Shen, New J. Phys. **12** 043048 (2010).
 - [26] Y. Shapir and X. R. Wang, Mod. Phys. Lett. B **4**, 1301(1990).
 - [27] D. R. Hofstadter, Phys. Rev. B **14**, 2239 (1976).
 - [28] D. J. Thouless, M Kohmoto, M. P. Nightingale and M. den Nijs, Phys. Rev. Lett. **49**, 405 (1982).
 - [29] M. Kohmoto, Ann. Phys. **160**, 343 (1985).
 - [30] B. I. Halperin, Phys. Rev. B **25**, 2185 (1982).
 - [31] C. Brüne, C. X. Liu, E. G. Novik, E. M. Hankiewicz, H. Buhmann, Y. L. Chen, X. L. Qi, Z. X. Shen, S. C. Zhang and L.W. Molenkamp, arXiv:1101.2627 (2011).
 - [32] S.D. Wang, Z. Z. Sun, G. Xiong, Y. Sun, and X. R. Wang, J. of Phys. A **37**, 1337-1343 (2004).
 - [33] S. Datta, *Electronic Transport in Mesoscopic Systems* (Cambridge University Press, Cambridge, U.K., 1995).
 - [34] D. Z. Liu, X. C. Xie and Q. Niu, Phys. Rev. Lett. **76**, 975 (1996).
 - [35] D. Guan, U. Ravaioli, R. W. Giannetta, M. Hannan, I. Adesida and M. R. Melloch, Phys. Rev. B **67**, 205328 (2003).